

Structuralization of Ca²⁺-Based Metal–Organic Frameworks Prepared via Coordination Replication of Calcium Carbonate

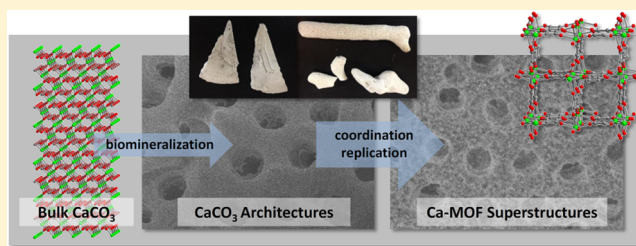
Kenji Sumida,^{†,‡} Ming Hu,^{†,§} Shuhei Furukawa,^{*,†} and Susumu Kitagawa^{*,†}

[†]Institute for Integrated Cell-Material Sciences (WPI-iCeMS), Kyoto University, Yoshida, Sakyo-ku, Kyoto 606-8501, Japan

[‡]Centre for Advanced Nanomaterials, School of Physical Sciences, The University of Adelaide, Adelaide, South Australia 5005, Australia

Supporting Information

ABSTRACT: The emergence of metal–organic frameworks (MOFs) as potential candidates to supplant existing adsorbent types in real-world applications has led to an explosive growth in the number of compounds available to researchers, as well as in the diversity of the metal salts and organic linkers from which they are derived. In this context, the use of carbonate-based precursors as metal sources is of interest due to their abundance in mineral deposits and their reaction chemistry with acids, resulting in just water and carbon dioxide as side products. Here, we have explored the use of calcium carbonate as a metal source and demonstrate its versatility as a precursor to several known frameworks, as well as a new flexible compound based on the 2,5-dihydroxybenzoquinone (H₂dhbq) linker, Ca(dhbq)(H₂O)₂. Furthermore, inspired by the ubiquity and unique structures of biomineralized forms of calcium carbonate, we also present examples of the preparation of superstructures of Ca-based MOFs via the coordination replication technique. In all, the results confirm the suitability of carbonate-based metal sources for the preparation of MOFs and further expand upon the growing scope of coordination replication as a convenient strategy for the preparation of structuralized materials.



INTRODUCTION

The design and synthesis of metal–organic frameworks¹ (MOFs) is an area that has experienced tremendous growth over the past decade, spurred in part by their potential utility in applications including gas storage, molecular separations, heterogeneous catalysis, drug delivery, and functional devices.² As opportunities for their industrial application emerge, optimization of their method of preparation is paramount in order to synthesize the materials in a form that not only maximizes their performance but also considers other aspects, including cost and environmental sustainability. With regard to the synthesis of the materials, the use of inexpensive and abundant precursors is certainly attractive, particularly if they are readily available within the framework of the current industrial infrastructure.

The conventional modular synthesis of MOF-based materials usually entails the complete dissolution of a metal source (generally a metal chloride or nitrate salt) and organic ligand within a polar organic solvent, followed by solvothermal treatment to afford the framework in the form of crystalline powders or single crystals. Recently, a variety of other inorganic metal precursors, including oxides and hydroxides, have received increased attention due to their enhanced processability in the macro- and mesoscopic length scales and ability to act as sacrificial templates for direct conversion into higher-order architectures of MOFs via the coordination replication method.³ For example, structuralized forms of copper

hydroxide⁴ have previously been employed in the generation of monolithic structures of microporous frameworks such as Cu₃(btc)₂ (HKUST-1; btc³⁻ = 1,3,5-benzenetricarboxylate),^{3g} Cu₂(bdc)₂(MeOH)₂ (bdc²⁻ = 1,4-benzenedicarboxylate), and Cu₂(bdc)₂(bpy) (bpy = 4,4'-bipyridine).³ⁱ Note that an additional advantage of such inorganic precursors is the benign reaction side products (e.g., water) that are generated in comparison to their halide and nitrate counterparts.

From this perspective, the use of carbonate-based metal precursors would carry similar advantages in processability and clean reactivity, although examples of their use have remained scarce in the literature. Under the acidic conditions employed for most MOF syntheses, it is anticipated that carbonates would readily participate in the framework formation, with the concomitant release of carbon dioxide and water as side products.



Among the metal carbonates, calcium carbonate is of particular interest owing to its occurrence in mineral deposits and wide industrial use. Furthermore, it is one of the most abundant biominerals, forming the skeletal component of many organisms, including shellfish and corals.⁵ These materials adopt highly complex, hierarchical structures that present a

Received: February 17, 2016

difficult challenge to mimic using conventional synthetic platforms. Herein, we explore the potential use of calcium carbonate as a precursor to MOF materials and look toward harnessing the unique structuralization of biomineralized forms of calcium carbonate as templates for the preparation of MOF superstructures. We first confirm its utility as a precursor by synthesizing bulk forms of known MOFs, followed by a new flexible MOF based on the 2,5-dihydroxybenzoquinone ($H_2d\text{hbq}$) linker. Then, we demonstrate the conversion of biomineralized calcium carbonate into structuralized MOF architectures via the coordination replication method.

EXPERIMENTAL SECTION

General Considerations. Unless otherwise stated, all reagents were obtained from commercial vendors and used without purification. All manipulations were carried out in the air, except for the handling of the activated forms of the frameworks in a nitrogen-filled glovebox. Solvothermal syntheses were carried out in a Yamato DKN302 constant-temperature oven within glass vials sealed with Teflon-lined lids. Microwave syntheses were carried out on a Biotage Initiator microwave reactor equipped with an infrared temperature sensor. Infrared spectra were collected in attenuated total reflectance (ATR) mode using a JASCO FT/IR-6100 spectrometer equipped with a TGS detector.

Field-Emission Scanning Electron Microscopy (FE-SEM). All observations were performed using a JEOL JSM-7001F4 microscope under an emission voltage of 15 kV. Samples were prepared either by deposition on glass slides by the drop-casting method or by adhesion on double-sided carbon tape, followed by coating with osmium nanoparticles to a thickness of 3 nm.

In Situ Powder X-ray Diffraction. All data were collected on a Rigaku Smartlab X-ray diffractometer equipped with a Cu $K\alpha$ source. The instrument was fitted with a custom-made variable-temperature sample stage with gas inlet and outlet ports for the flow of controlled gas compositions. The inlet side was connected to a BELFlow vaporizer apparatus (BEL Japan, Inc.) using a He carrier gas (flow rate 100 cm^3/min) and distilled water as the vapor source. In a typical experiment, a solvated sample was first activated on the sample stage under a dry He flow, and the humidity of the flow gas was then sequentially increased in a stepwise fashion via the BELFlow-1 version 1.00 software package.

[Ca(dhbq)(H_2O) $_2$] $\cdot H_2O$ (1 $\cdot H_2O$). In a 20 mL glass vial equipped with a magnetic stirrer bar, calcium carbonate (150 mg, 1.50 mmol) was added to a vigorously stirred suspension of $H_2d\text{hbq}$ (210 mg, 1.50 mmol) in water (10 mL). The vial was capped, and the mixture was stirred overnight at room temperature. After this time, a crimson suspension was obtained, which was filtered off and washed with water (3×20 mL) followed by dichloromethane (3×20 mL). The resulting powder was dried in vacuo at 80 $^\circ\text{C}$ for a period of 12 h to afford 1 $\cdot H_2O$ as a dark red powder (275 mg, 69%). Anal. Calcd for $C_6H_6O_6Ca \cdot 0.1H_2O$: C, 33.36; H, 2.89. Found: C, 33.22; H, 2.74. IR (neat): 3270 (m br), 1668 (w), 1641 (w), 1594 (w), 1502 (s), 1387 (s), 1259 (s), 825 (m) cm^{-1} . Single crystals of the compound could be prepared by heating the same aqueous reaction mixture to 60 $^\circ\text{C}$ under static conditions for a period of 3 days. Crystallographic data for 1 $\cdot H_2O$ have been deposited with the Cambridge Crystallographic Data Centre (CCDC) under accession code 1447832. These data can be obtained free of charge from the Cambridge Crystallographic Data Centre via www.ccdc.cam.ac.uk/data_request/cif.

Coordination Replication Experiments. In a typical experiment, a biomineralized calcium carbonate sample derived from *Baculogyphina sphaerulata* was first immersed in a mixed aqueous solution of sodium hydroxide and sodium hypochlorite in order to remove trace organic materials from the structures. After they were rinsed with distilled water (5×100 mL), the samples were further immersed in distilled water for 24 h. Then, the sample was transferred to an aqueous solution containing an excess of $H_2\text{sq}$ and heated in a microwave reactor at 120 $^\circ\text{C}$ for 3, 6, 9, or 12 h. After the replication process, the

samples were washed by immersion in distilled water and dried in the air in an oven set to a temperature of 100 $^\circ\text{C}$.

RESULTS AND DISCUSSION

Preparation of Ca^{2+} -Based Frameworks. In order to investigate the appropriate reactivity of calcium carbonate as a precursor for the assembly of metal–organic frameworks, several ditopic linkers known to form Ca^{2+} -based frameworks, namely 1,4-benzenedicarboxylate ($H_2\text{bdc}$), 2,5-dihydroxy-1,4-benzenedicarboxylate ($H_4\text{dobdc}$), and squaric acid ($H_2\text{sq}$), were first tested. Here, the reaction conditions were screened using a microwave reactor, varying the solvent composition, reaction temperature, and reaction time. Despite its low solubility in all of the solvent combinations tested, calcium carbonate was found to form highly crystalline products, leading to the successful isolation of the $Ca(\text{bdc})(H_2O)_3$ (Figure 1A and Figure S1 in the Supporting Information),⁶

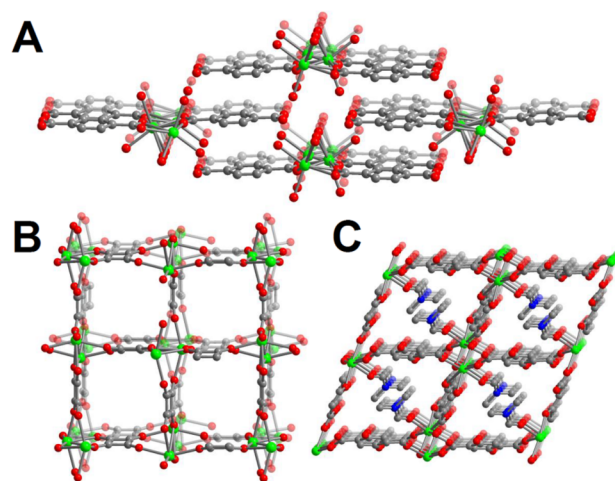


Figure 1. Portions of the single-crystal structures of (A) $Ca(\text{bdc})(H_2O)_3$ as viewed along the crystallographic c axis,⁶ (B) $Ca(\text{sq})(H_2O)$ as viewed along the crystallographic c axis,⁷ and (C) $Ca(H_2\text{dobdc})(\text{DMF})$ as viewed along the crystallographic a axis.⁸ Green, gray, blue, and red spheres represent Ca, C, N, and O atoms, respectively, while H atoms and extraframework water molecules have been omitted in panel B for clarity.

$Ca(\text{sq})(H_2O)$ (Figure 1B and Figure S2 in the Supporting Information),⁷ and $Ca(H_2\text{dobdc})(\text{DMF})$ (Figure 1C and Figure S3 in the Supporting Information) frameworks⁸ with complete consumption of the metal source.

Synthesis and Characterization of $Ca(\text{dhbq})(H_2O)_2$. The successful use of calcium carbonate in the synthesis of the frameworks noted above prompted efforts toward the synthesis of frameworks possessing greater porosity. Here, the 2,5-dihydroxybenzoquinone linker ($H_2d\text{hbq}$; Figure 2) was targeted due to its structural similarity with the squarate anion employed in the synthesis of $Ca(\text{sq})(H_2O)$, while

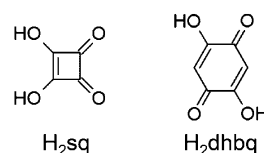


Figure 2. Molecular structures of squaric acid ($H_2\text{sq}$) and 2,5-dihydroxybenzoquinone ($H_2d\text{hbq}$) employed in this work.

potentially providing a greater distance between Ca^{2+} -based chains (and consequently a greater pore wall separation). A number of extended framework materials have previously been reported using the $\text{d}(\text{hbq})^{2-}$ linker,⁹ although these reports have been limited to compounds based on the transition-metal elements.

The solvated form of $\text{Ca}(\text{d}(\text{hbq}))(\text{H}_2\text{O})_2$ ($1 \cdot \text{H}_2\text{O}$) was obtained via the addition of calcium carbonate to an aqueous solution of $\text{H}_2\text{d}(\text{hbq})$, followed by heating at 60°C for a period of 3 days.¹⁰ After this time, red-brown block-shaped single crystals suitable for diffraction studies were obtained from the walls of the reaction vessel. X-ray analysis revealed a monoclinic crystal system (space group $C2/m$) consisting of an extended network structure exhibiting narrow, one-dimensional pores (see Figure 3A). Consistent with its diffuse, oxophilic nature,

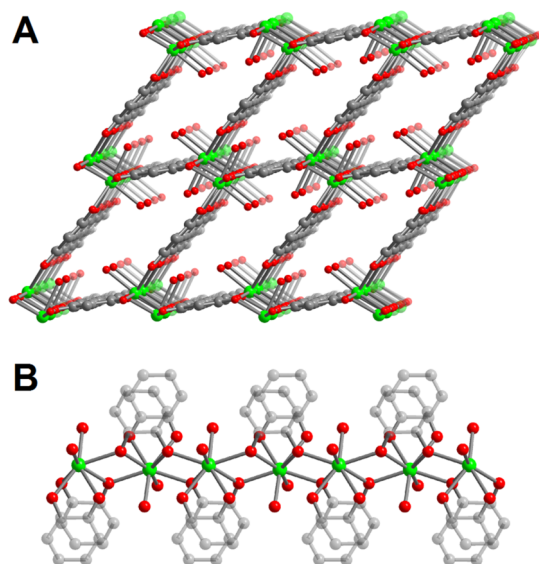


Figure 3. (A) Portion of the single-crystal structure of $\text{Ca}(\text{d}(\text{hbq}))(\text{H}_2\text{O})_2$ (**1**), as viewed along the crystallographic b axis, and (B) a side-on view of the one-dimensional Ca^{2+} -based chains within the structure. Green, gray, and red spheres represent Ca, C, and O atoms, respectively, while H atoms have been omitted for clarity.

the individual Ca^{2+} ions reside in an eight-coordinate, distorted-square-antiprismatic ligand geometry, wherein six coordination sites are occupied by $\text{d}(\text{hbq})^{2-}$ oxygen atoms, and a further two water molecules projecting into the pores to complete the coordination sphere. A total of three $\text{d}(\text{hbq})^{2-}$ half-units are bound to each Ca^{2+} metal center, one of which is coordinated in a chelating fashion, while the other two are disposed such that the oxygen atoms bridge adjacent Ca^{2+} cations to form a zigzag shaped one-dimensional chain (see Figure 3B). Neighboring chains are linked via opposite ends of the $\text{d}(\text{hbq})^{2-}$ linker to form diamond-shaped cavities of ca. 3.7 \AA between opposing walls (based on van der Waals radii) that are populated by hydrogen-bonded water molecules originating from the synthesis solvent (four per unit cell).

The stability of $1 \cdot \text{H}_2\text{O}$ toward evacuation of both the bound and unbound water molecules within the pores was probed using a combination of powder X-ray diffraction studies and thermogravimetric analysis. A comparison of the diffraction data collected for an as-synthesized sample revealed an excellent match with that of the simulated diffraction pattern from the single-crystal structure of $1 \cdot \text{H}_2\text{O}$ (see Figure 4).

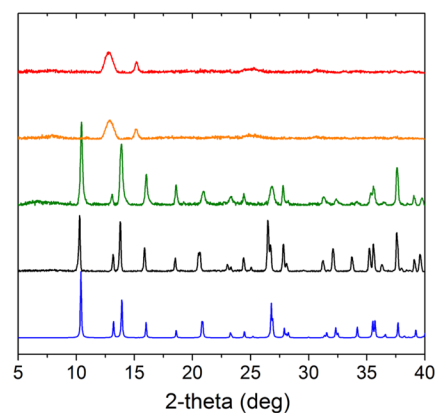


Figure 4. Simulated powder X-ray diffraction pattern from the single-crystal structure of solvated **1** (blue) and experimental data collected under a dry He flow for an as-synthesized sample at 25°C (black) and after the sample temperature was raised to 100°C (green), 140°C (orange), and 180°C (red).

Heating of the powder sample under a He flow to 100°C resulted in a slight shift of the diffraction peaks to higher angles, which is consistent with a slight contraction of the unit cell dimensions. Interestingly, the peak intensities dramatically diminished at higher temperatures of 140°C and above, resulting in a new, high-temperature phase of poorer crystallinity exhibiting two prominent peaks at 2θ values of ca. 12.9° and 15.1° with relatively broad peak profiles. Meanwhile, the thermogravimetric data (Figure S4 in the Supporting Information) indicated a weight loss attributable to the gradual loss of one (extraframework) water molecule per formula unit up to 140°C , suggesting the structural change results as a result of the liberation of a water molecule from the pores.¹¹ The first prominent peak of the high-temperature phase corresponds to a crystal lattice d spacing of 6.9 \AA , which correlates closely with the distance of 7.1 \AA between adjacent Ca^{2+} chains bridged by the $\text{d}(\text{hbq})^{2-}$ ligands, as calculated by an averaging of the $\text{Ca}\cdots\text{Ca}$ distances. This suggested that the loss of long-range order in the sample was due to the collapse of the one-dimensional pores upon evacuation of the extraframework water molecules, rather than the decomposition of the framework via the breaking of the coordination bonds.

In order to test this hypothesis, in situ powder X-ray diffraction experiments were performed under a He flow containing variable water concentrations. Figure 5 shows data stemming from an activated sample of **1** first placed under a pure He flow at 25°C (red), which was then subjected a gas stream containing successively higher concentrations of water vapor. Relatively minor changes to the diffraction pattern are observed up to a relative pressure of 0.6, including a slight shift of the major peaks to lower angles together with a sharpening of the peaks, presumably due to a slightly enhanced long-range order of the high-temperature phase. Further increases in the water composition of the gas flow resulted in a return to the original crystalline phase of $1 \cdot \text{H}_2\text{O}$, confirming that the transition between the low- and high-temperature phases is reversible.¹² A water adsorption isotherm collected at 298 K (Figure 6) further confirmed the affinity of the pores of activated **1** toward water, wherein the step observed at $P/P_0 = 0.7$ is in good agreement with the observations from the in situ powder X-ray diffraction experiments. Note that low-pressure adsorption data collected for N_2 (77 K) and CO_2 (298 K) resulted in no uptake, suggesting that the initial population of

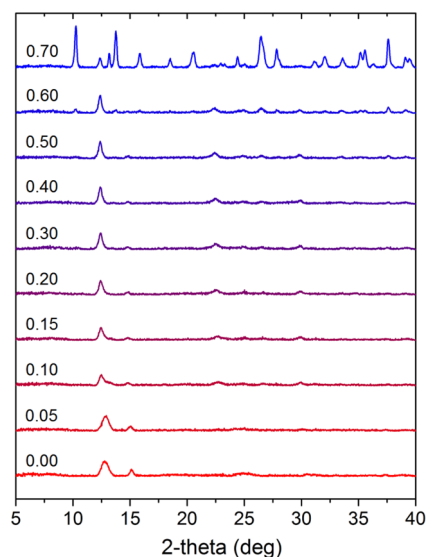


Figure 5. Evolution of the powder X-ray diffraction pattern collected for an activated sample of **1** upon exposure to increasing levels of humidity. The fraction associated with each plot represents the relative pressure of water (P/P_0) in the gas mixture.

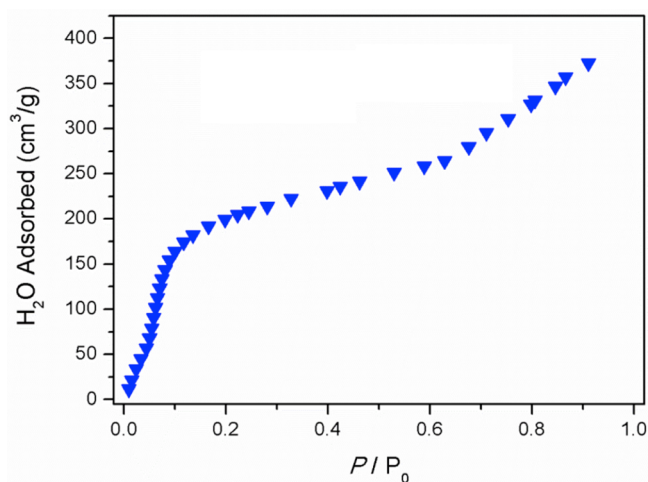


Figure 6. H_2O adsorption isotherm collected at 298 K for an activated sample of **1**.

the pores with water molecules is required for the observed structural transition. Further, the exposure of activated **1** to larger coordinating solvent molecules (e.g., methanol, ethanol, acetone, and acetonitrile) did not induce a return to the original crystalline phase, which is a result of the small cavity size (ca. 3.7 Å) in comparison to the kinetic diameter of these solvent molecules.

Coordination Replication of Biomineralized Calcium Carbonate. The low solubility of calcium carbonate in water and organic solvents and high reactivity toward the organic linkers tested above suggested that structuralized forms of the metal precursor would be ideal for the fabrication of superstructures of Ca^{2+} -based frameworks. In this context, biomineralized forms of calcium carbonate are ubiquitous in nature, and many feature extraordinary, hierarchically porous architectures that are optimized for their particular functions.⁵ While examples of the fabrication of materials that replicate such complex structures have remained rare, one elegant study utilized the ordered skeletal plate of a sea urchin to template

periodically structured macroporous copper via a two-step procedure.¹³ This involved the initial generation of a polymer cast representing an exact negative of the template¹⁴ and dissolution of the calcium carbonate under acidic conditions, followed by electrochemical deposition of the copper metal into the voids of the polymer scaffold. In our work, we focused on the direct use of the biomineral template as a sacrificial material and conversion into the MOF architectures via the coordination replication method.

The Foraminifera, which are organisms that mostly reside on or within the sediment bed of the seafloor, feature tests (shells) constructed from calcium carbonate that in many cases can possess tremendously elaborate structures. Here, we obtained a sample of *Baculogypsina sphaerulata*¹⁵ (Figure 7A; “star sand”)

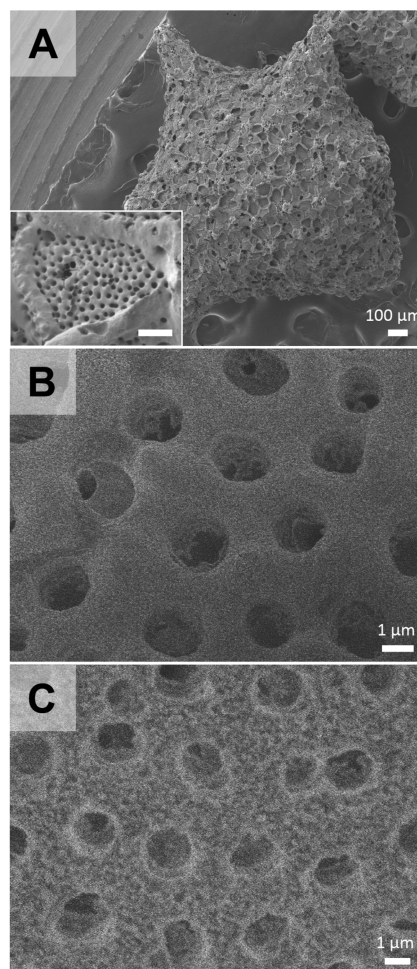


Figure 7. Field-emission SEM images of (A) a biomineralized calcium carbonate sample derived from *Baculogypsina sphaerulata*¹⁵ (“star sand”) (the inset gives an enlarged view of the macroporous features on the surface) and enlarged views of the macropores (B) before and (C) after microwave treatment for 12 h at 120 °C in an aqueous solution containing H_2sq . The scale bar within the inset corresponds to 10 μm.

from Hoshizuna-no-hama (“Star Sand Beach”), Iriomote Island, Okinawa, Japan, which possesses a star-shaped shell approximately 1.5 mm in size. Closer inspection of the surface of the structure indicated the presence of higher order patterning at the surface and the presence of a high density of macropores approximately 1 μm in diameter (Figure 7B). Analysis of the powder X-ray diffraction pattern of a ground form of the

sample revealed its composition to be a moderately crystalline form of calcite (see Figure S8 in the Supporting Information), which corresponds to the form of calcium carbonate used successfully in the bulk MOF syntheses.

Encouraged by the composition of the materials, residual organic matter, such as proteins, was first removed by dissolution under basic conditions. After washing and drying of the samples, the sample was placed in an aqueous solution of H_2sq (15 mM) heated to 120 °C for 12 h. After this time, SEM revealed a significantly rougher macropore morphology and the presence of rodlike crystallites embedded on the surface of the material (Figure 7C). Powder X-ray diffraction data (Figure S8 in the Supporting Information) confirmed the partial conversion of the calcium carbonate to a highly crystalline $\text{Ca}(\text{sq})(\text{H}_2\text{O})$ phase, with the original calcite reflections still present following the replication process. Interestingly, longer reaction times did not lead to full conversion but resulted in the formation of large, rodlike single crystals of $\text{Ca}(\text{sq})(\text{H}_2\text{O})$ up to 500 μm in length (Figure S9 in the Supporting Information). The propensity for bulk crystallization to occur suggests the relatively fast dissolution of the calcium carbonate phase relative to the formation of the $\text{Ca}(\text{sq})(\text{H}_2\text{O})$ phase. Furthermore, a large volume increase of approximately 2.9 times (based on the density of Ca^{2+} ions in single-crystal structures of calcite and the $\text{Ca}(\text{sq})(\text{H}_2\text{O})$ framework) is expected to limit the internal space available for crystal growth within the structures, leading to a preference for the Ca^{2+} ions to diffuse out into the bulk solution as the intrinsic porosity is diminished. Similar tendencies for bulk crystallization to occur were observed for other types of biomineralized calcium carbonate samples, including those derived from marine corals (Figure S10 in the Supporting Information), sea urchin skeletal plates (Figure S11 in the Supporting Information), and egg shells (Figure S12 in the Supporting Information).

CONCLUSIONS AND FUTURE OUTLOOK

The foregoing has discussed the use of calcium carbonate as a versatile metal source for the formation of Ca^{2+} -based MOFs. Its high reactivity toward organic acids facilitated the formation of highly crystalline samples of several known frameworks, as well as a new framework based on the H_2dnhq linker $\text{Ca}(\text{dnhq})(\text{H}_2\text{O})_2$, possessing a flexible structure based on the reversible adsorption of water molecules. Importantly, the low solubility of calcium carbonate in the conventional solvents used in MOF synthesis allowed biomineralized samples to be partially converted with retention of the original architecture, offering a new route to hierarchically structuralized MOFs adopting the morphologies of functional biominerals. Furthermore, this work has further underscored the versatility of the coordination replication technique, and future studies will be directed toward the more effective use of the unique structures of biomineralized materials for the preparation of functional MOF-based architectures.

ASSOCIATED CONTENT

Supporting Information

The Supporting Information is available free of charge on the ACS Publications website at DOI: 10.1021/acs.inorgchem.6b00397.

Full experimental procedures, powder X-ray diffraction data, thermogravimetric analysis data, adsorption isotherms, and scanning electron microscopy data (PDF)

Crystallographic data for $1 \cdot \text{H}_2\text{O}$ (CIF)

AUTHOR INFORMATION

Corresponding Authors

*E-mail for S.F.: shuhei.furukawa@icems.kyoto-u.ac.jp.

*E-mail for S.K.: kitagawa@icems.kyoto-u.ac.jp.

Present Address

[§]Department of Physics, East China Normal University, Shanghai 200241, People's Republic of China.

Notes

The authors declare no competing financial interest.

ACKNOWLEDGMENTS

K.S. is grateful to the JSPS Postdoctoral Fellowship Program for Foreign Researchers and the Australian Research Council for funding (DE160100306). This work was supported by a Grant-in-Aid for Scientific Research (15H03785 (S.F.)) from the MEXT of Japan. iCeMS is supported by the World Premier International Research Initiative (WPI), MEXT of Japan. The authors thank CeMI for assistance with electron microscopy, Dr. M. Nakahama for experimental assistance, and Dr. C. J. Sumbly and Ms. N. Shimanaka for helpful discussions.

REFERENCES

- (1) (a) Yaghi, O. M.; O'Keeffe, M.; Ockwig, N. W.; Chae, H. K.; Eddaoudi, M.; Kim, J. *Nature* **2003**, *423*, 705–714. (b) Kitagawa, S.; Kitaura, R.; Noro, S. *Angew. Chem., Int. Ed.* **2004**, *43*, 2334–2375. (c) Férey, G. *Chem. Soc. Rev.* **2008**, *37*, 191–214.
- (2) Metal–organic frameworks were the topic of recent special themed issues in *Chem. Rev.* and *Chem. Soc. Rev.*: (a) Zhou, H.-C.; Long, J. R.; Yaghi, O. M. *Chem. Rev.* **2012**, *112*, 673–674. (b) Zhou, H.-C.; Kitagawa, S. *Chem. Soc. Rev.* **2014**, *43*, 5415–5418.
- (3) (a) Reboul, J.; Furukawa, S.; Horike, N.; Tsotsalas, M.; Hirai, K.; Uehara, H.; Kondo, M.; Louvain, N.; Sakata, O.; Kitagawa, S. *Nat. Mater.* **2012**, *11*, 717–723. (b) Stassen, I.; Campagnol, N.; Fransaer, J.; Vereecken, P.; De Vos, D.; Ameloot, R. *CrystEngComm* **2013**, *15*, 9308–9311. (c) Zhan, W.; Kuang, Q.; Zhou, J.; Kong, X.; Xie, Z.; Zheng, L. *J. Am. Chem. Soc.* **2013**, *135*, 1926–1933. (d) Khaletskaia, K.; Reboul, J.; Meilikhov, M.; Nakahama, M.; Diring, S.; Tsujimoto, M.; Isoda, S.; Kim, J.; Kamei, K.; Fischer, R. A.; Kitagawa, S.; Furukawa, S. *J. Am. Chem. Soc.* **2013**, *135*, 10998–11005. (e) Liu, Y.; Zhang, W.; Li, S.; Cui, C.; Wu, J.; Chen, H.; Huo, F. *Chem. Mater.* **2014**, *26*, 1119–1125. (f) Nakahama, M.; Reboul, J.; Kamei, K.; Kitagawa, S.; Furukawa, S. *Chem. Lett.* **2014**, *43*, 1052–1054. (g) Moitra, N.; Fukumoto, S.; Reboul, J.; Sumida, K.; Zhu, Y.; Nakanishi, K.; Furukawa, S.; Kitagawa, S.; Kanamori, K. *Chem. Commun.* **2015**, *51*, 3511–3514. (h) Reboul, J.; Yoshida, K.; Furukawa, S.; Kitagawa, S. *CrystEngComm* **2015**, *17*, 323–330. (i) Sumida, K.; Moitra, N.; Reboul, J.; Fukumoto, S.; Nakanishi, K.; Kanamori, K.; Furukawa, S.; Kitagawa, S. *Chem. Sci.* **2015**, *6*, 5938–5946. (j) Zhao, J.; Nunn, W. T.; Lemaire, P. C.; Lin, Y.; Dickey, M. D.; Oldham, C. J.; Walls, H. J.; Peterson, G. W.; Losego, M. D.; Parsons, G. N. *J. Am. Chem. Soc.* **2015**, *137*, 13756–13759.
- (4) Fukumoto, S.; Nakanishi, K.; Kanamori, K. *New J. Chem.* **2015**, *39*, 6771–6777.
- (5) Mann, S. *Biomineralization: Principles and Concepts in Bioinorganic Materials Chemistry*; Oxford University Press: Oxford, U.K., 2001.
- (6) Matsuzaki, T.; Iitaka, Y. *Acta Crystallogr., Sect. B: Struct. Crystallogr. Cryst. Chem.* **1972**, *28*, 1977–1981.
- (7) (a) Robl, C.; Weiss, A. *Mater. Res. Bull.* **1987**, *22*, 373–380. (b) Horike, S.; Kamitsubo, Y.; Inukai, M.; Fukushima, T.; Umeyama, D.; Itakura, T.; Kitagawa, S. *J. Am. Chem. Soc.* **2013**, *135*, 4612–4615.
- (8) Liang, P.-C.; Liu, H.-K.; Yeh, C.-T.; Lin, C.-H.; Zima, V. *Cryst. Growth Des.* **2011**, *11*, 699–708.
- (9) (a) Abrahams, B. F.; Hudson, T. A.; McCormick, L. J.; Robson, R. *Cryst. Growth Des.* **2011**, *11*, 2717–2720. (b) Darago, L. E.; Aubrey,

M. L.; Yu, C. J.; Gonzalez, M. I.; Long, J. R. *J. Am. Chem. Soc.* **2015**, *137*, 15703–15711.

(10) The reaction of other metal salts, such as $\text{CaCl}_2 \cdot 4\text{H}_2\text{O}$ and $\text{Ca}(\text{NO}_3)_2 \cdot 4\text{H}_2\text{O}$, using similar reaction conditions resulted in amorphous and low-crystallinity samples, and these solids were not characterized further.

(11) Further heating of the sample above 450 °C resulted in a large transition whose magnitude is consistent with the loss of the $\text{d}^{\text{hbq}}^{2-}$ linker from the solid, resulting in the decomposition of the framework.

(12) Note that the alternative rehydration pathway of dissolution and recrystallization would require the presence of a solid–fluid interface, which is not present in the case of a framework placed under a hydrated gas stream. Furthermore, while immersion of a similarly activated material in liquid water also immediately restored the original $1 \cdot \text{H}_2\text{O}$ phase (see Figure S7 in the Supporting Information), this could not be achieved in other solvents such as methanol. This further suggests that the restoration of the low-temperature phase occurs due to water migrating back into the pores.

(13) Lai, M.; Kulak, A. N.; Law, D.; Zhang, Z.; Meldrum, F. C.; Riley, D. J. *Chem. Commun.* **2007**, 3547–3549.

(14) Yue, W.; Park, R. J.; Kulak, A. N.; Meldrum, F. C. *J. Cryst. Growth* **2006**, *294*, 69–77.

(15) World Foraminera Database: *Baculogypsina sphaerulata*; <http://www.marinespecies.org/foraminifera/aphia.php?p=taxdetails&id=484702> (accessed January 30, 2016).